

UNIFYING DISENTANGLED REPRESENTATION LEARNING WITH COMPOSITIONAL BIAS

Anonymous authors

Paper under double-blind review

ABSTRACT

Existing disentangled representation learning methods rely on inductive biases tailored for the specific factors of variation (e.g., attributes or objects). However, these biases are incompatible with other classes of factors, limiting their applicability for disentangling general factors of variation. In this paper, we propose a unified framework for disentangled representation learning, accommodating both attribute and object disentanglement. To this end, we reformulate disentangled representation learning as maximizing the compositionality of the latents. Specifically, we randomly *mix* two latent representations from distinct images and maximize the likelihood of the resulting composite image. Under this general framework, we demonstrate that adjusting the strategy for mixing between two latent representations allows us to capture either attributes or objects within a single framework. To derive appropriate mixing strategies, we analyze the compositional structures of both attributes and objects, then incorporate these structures into their respective mixing strategies. Our evaluations show that our method achieves performance that matches or exceeds strong baselines in both attribute and object disentanglement.

1 INTRODUCTION

Understanding the underlying structure of data is crucial for building robust and interpretable machine learning models. In particular, by perceiving the world through compositional concepts, unseen data can be decomposed into simpler, more interpretable components. This approach dramatically improves data efficiency of learning, as unseen data can be explained as combinations of already learned concepts (Lake et al., 2017; Kuo et al., 2021). In this context, disentangled representation learning (Higgins et al., 2018; Bengio & LeCun, 2007) aims to decompose the data into its underlying factors of variation. As Locatello et al. (2019) theoretically proves that disentangled representation learning cannot be achieved without inductive biases or direct supervision, the field has focused on designing appropriate inductive biases to disentangle desirable factors in an unsupervised manner.

Attribute and object disentanglement are two of the most common tasks in disentangled representation learning. Attribute disentanglement (Burgess et al., 2017; Chen et al., 2016; Kim & Mnih, 2018; Chen et al., 2018; Ren et al., 2022) aims to isolate various features or properties of the data. Disentanglement between latent variables is often encouraged by additional regularization terms, such as minimizing Total Correlation in VAEs (Burgess et al., 2017; Kim & Mnih, 2018; Chen et al., 2018), maximizing mutual information between latents and images Chen et al. (2016); Lin et al. (2020b), or minimizing mutual information between vector-wise latents (Yang et al., 2023). On the other hand, object-centric learning focuses on decomposing scenes into individual objects (Burgess et al., 2019; Greff et al., 2019; Engelcke et al., 2020; Locatello et al., 2020; Jiang et al., 2023). These methods rely on a spatial exclusiveness bias, where each pixel in an image must correspond to a unique object, implemented within model architectures such as spatial-attention masks (Burgess et al., 2019; Engelcke et al., 2020), pixel-mixture decoders (Greff et al., 2019), or slot attention (Locatello et al., 2020).

While both attribute and object disentanglement share the common goal of identifying underlying factors of variation, the aforementioned inductive biases are crafted specific to their respective target factors and are incompatible with each other. Moreover, relying on these inductive biases may limit their extension to disentangling general factors of variation or scenarios that involve both attributes and objects in a scene. This challenge motivates us to develop a unified inductive bias capable of capturing a broader range of factors of variation.

In this paper, we present a unified framework for disentangled representation learning that supports both attribute and object disentanglement. Inspired by the fact that the goal of disentangled representation learning is to achieve combinatorial generalization, we formulate disentangled representation learning as the process of maximizing compositionality and carefully design the composition rule that ensures valid combinations of latents. Specifically, we randomly compose two latent representations from different images and maximize the likelihood of the resulting composite images. Based on the different compositional structures of attributes and objects, we derive specific mixing strategies for attribute and object disentanglement that inform a valid composition between latents. Unlike previous methods, which introduce inductive biases tailored specifically to either attribute or object disentanglement and are not compatible with both, our framework is compatible with both types of factors. Our experiments show that our framework effectively disentangles both attributes and objects by adjusting only the mixing strategy, without altering model architectures or objective functions.

Our contributions are as follows: (1) We present a unified framework for disentangled representation learning that effectively addresses both attribute and object disentanglement. (2) We derive simple yet effective mixing strategies for disentangling attributes or objects, drawing from their underlying compositional structures. (3) We compare our methods with strong baselines specifically designed for disentangled representation learning and object-centric learning and verifies that our method can achieve comparable or even superior performance to the baselines.

2 BACKGROUNDS : DISENTANGLED REPRESENTATION LEARNING

In this section, we briefly review the two main streams of disentangled representation learning: attribute and object disentanglement. We discuss how previous methods have achieved disentanglement and why they are incompatible to each other. More in-depth discussions on related works are presented in Appendix A.1.

Attribute disentanglement In attribute disentanglement, scenes are assumed to consist of a fixed number of random variables (Kim & Mnih, 2018). Typical approaches aim to discover independent latent variables by designing objective functions that promote their statistical independence. For instance, (Burgess et al., 2017; Kim & Mnih, 2018; Chen et al., 2018) use Total Correlation (Watanabe, 1960) within the VAE framework to assess independence between latent dimensions. Alternatively, (Lin et al., 2020b; Ren et al., 2022) introduce contrastive regularization, encouraging variations in each latent variable to produce distinct changes in the output space of GANs. Recently, Yang et al. (2023) proposed minimizing the upper bound of mutual information between latent variables. These *information-theoretic objectives* are suited for scenarios where each data is composed of a fixed set of factors, with each latent variable corresponding to a specific factor. However, when this assumption is violated, defining and directly measuring independence between latent variables becomes non-trivial. For example, in object-centric scenes, the same objects can appear in different spatial locations, complicating the definition of independence metrics for object representations.

Object disentanglement In object-centric learning, random variables are assumed to be independent but share a generative mechanism, such that different orderings of the latents still produce identical images (Greff et al., 2019). Since measuring independence between object representations is challenging, object-centric approaches use architectural biases to promote independence indirectly. Early methods implemented spatial exclusiveness through decoders that renders each latent into pairs of a RGB image and a mask, blending them to form the final output (Burgess et al., 2019; Greff et al., 2019; Engelcke et al., 2020; Lin et al., 2020a). Each mask corresponds to a distinct region, inducing spatial exclusivity among the latents. Slot attention (Locatello et al., 2020) adopts a spatially exclusive mechanism within the encoder, where each latent (slot) exclusively binds to spatial locations in the input images. These *spatial exclusive biases* constrain each latent to bind to non-overlapping spatial regions, and the auto-encoding objective encourages the encoder to cluster spatially correlated pixels. While these biases facilitate the disentangling of spatial factors, they restrict the ability to disentangle non-spatial factors like attributes.

In summary, we identify two distinct inductive biases that promote independence between latent variables, either directly or indirectly. As these biases are tailored specific to each class of factors of variation (*i.e.*, attributes and objects), they are not only incompatible with each other but also

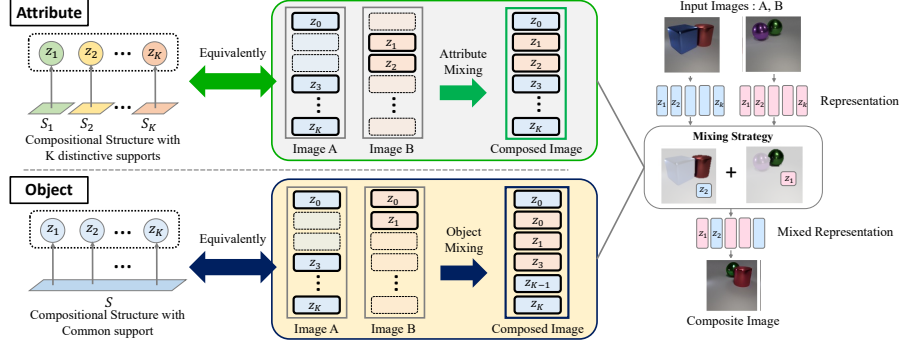


Figure 1: Overview of our method. We introduce a unified framework for disentangled representation learning, which is compatible with both attribute and object disentanglement. To this end, we formulate our learning framework as randomly composing latents from two distinct images, and maximize the likelihood of resulting composite images (Section 3.1). To disentangle attribute and object within this framework, we devise two specific mixing strategies to properly reflect their compositional structures (Section 3.2). Finally, we maximize the likelihood of composite images and ensure compositional consistency (Section 3.3).

challenging to extend to disentangling general factors of variation. This challenge motivates us to seek a unified approach that can accommodate both attribute and object disentanglement.

3 UNIFYING DISENTANGLED REPRESENTATION LEARNING WITH COMPOSITIONAL BIAS

Our goal is to develop a unified framework for disentangled representation learning, which is compatible with both attribute and object disentanglement. In the following sections, we illustrate the overall framework to handle both attribute and object disentanglement (Section 3.1) and how we derive our new inductive bias from the different compositional structures of each factor of variation (Section 3.2). Finally, we demonstrate how we design the learning objectives to instantiate this general framework (Section 3.3). Figure 1 summarizes the overall framework of our method.

3.1 UNIFIED FRAMEWORK FOR LEARNING DISENTANGLED REPRESENTATION

Disentangled representation learning aims to represent an image $\mathbf{x} \in \mathbb{R}^{H \times W \times C}$ into a set of K latent representations $\mathbf{z} = \{\mathbf{z}_i\}_{i=1}^K$, where each latent $\mathbf{z}_i \in \mathbb{R}^d$ is expected to capture independent factors of variation. Previous approaches achieve this goal by utilizing specific assumptions about the latent representations, such as statistical independence (Kim & Mnih, 2018; Chen et al., 2018) or spatial exclusiveness (Greff et al., 2019; Locatello et al., 2020) between the latent variables. Such assumptions are specific to type of factors of variation (e.g., attributes or objects) and imposed by tailored architecture or regularization, making them incompatible with different types of disentanglement.

Instead, we propose to employ the maximization of *compositionality* in the representation as a general objective for disentanglement learning while instantiating various disentanglement structures by controlling *only* the composition operator. To this end, we follow (Jung et al., 2024) by randomly composing latent representations from two images and maximizing the likelihood of the resulting composite image. Specifically, given two images $\mathbf{x}^1, \mathbf{x}^2 \sim p(\mathbf{x})$ and their representations $\mathbf{z}^1, \mathbf{z}^2 \in \mathbb{R}^{K \times d}$, respectively, we produce their composite representation \mathbf{z}^c by some composition operator. Then, we decode \mathbf{z}^c into a composite image \mathbf{x}^c and maximize its likelihood $p(\mathbf{x}^c)$ to ensure the production of realistic images by:

$$\theta^* = \arg \max_{\theta} p(\mathbf{x}^c) = \arg \max_{\theta} p(D_{\phi}(\pi(\mathbf{z}^1, \mathbf{z}^2))) = \arg \max_{\theta} p(D_{\phi}(\pi(E_{\theta}(\mathbf{x}^1), E_{\theta}(\mathbf{x}^2))))), \quad (1)$$

where E_{θ}, D_{ϕ} denote an encoder and a decoder, respectively. $\pi(\cdot, \cdot)$ represents a mixing operation between two sequences of representations such that $\pi(\mathbf{z}^1, \mathbf{z}^2) = \{\mathbf{z}_i^c \mid \mathbf{z}_i^c = \mathbf{z}_{\sigma_i}^{r_i}, i \in \{1, \dots, K\}\}$, where $r_i \in \{1, 2\}$ indicates whether the i -th element is selected from \mathbf{z}^1 or \mathbf{z}^2 , and $\sigma_i \in \{1, \dots, K\}$

is an index that determines the order. Note that this formulation does not impose any assumptions specific to the factors of variation on the latent space. While (Jung et al., 2024) relies on architectural bias (*i.e.*, slot attention) and focused on improving object representation by maximizing compositionality, we argue that various factorization structure of latent can be imposed by designing how two latents are composed through the mixing operator $\pi(\cdot, \cdot)$. In the following section, we will demonstrate how we derive specific mixing operator $\pi(\cdot, \cdot)$ —referred to as the *mixing strategy*—for two representative examples of factors of variation: attributes and objects.

3.2 MIXING STRATEGY FOR REFLECTING THE COMPOSITIONAL STRUCTURE

The mixing strategy is defined to produce a random composition between two sequences of latent representations: $\mathbf{z}^1, \mathbf{z}^2$. It is important to note that not all random compositions result in valid outcomes. For instance, when we mix the ground-truth factors of face attributes, the composition having two noses becomes an invalid composition. This is because ground-truth factors follow a certain structure to be composed into a complete image, which we refer to as the *compositional structure* of factors of variation. Therefore, we characterize the compositional structure of each factors of variation, and derive corresponding mixing strategy. We start by defining disentangled representation, following (Roth et al., 2023).

Definition 1 (Disentanglement with a factorized support). Let us denote the support of $p(\mathbf{x})$ as $\mathcal{S}(p(\mathbf{x})) = \{\mathbf{x} | p(\mathbf{x}) > 0\}$. Given a sequence of random vectors $\mathbf{z} = \{\mathbf{z}_i\}_{i=1}^K$, \mathbf{z} is *disentangled with a factorized support* if $\mathcal{S}(p(\mathbf{z})) = \mathcal{S}(p(\mathbf{z}_1)) \times \mathcal{S}(p(\mathbf{z}_2)) \times \cdots \times \mathcal{S}(p(\mathbf{z}_K)) \stackrel{\text{def}}{=} \mathcal{S}^\times(p(\mathbf{z}))$, where \times denotes Cartesian product.

Note the factorized support implies that for any composition of \mathbf{z}_i independently encoded from multiple images, there must exist some real image \mathbf{x} represented by \mathbf{z} , aligning with our formulation. To achieve the disentangled representation, following the definition, we design mixing strategies that achieve $q_\theta(\mathbf{z} | \mathbf{x})$ that the aggregate distribution $\bar{q}_\theta(\mathbf{z}) = \mathbb{E}_{\mathbf{x}}[q_\theta(\mathbf{z} | \mathbf{x})]$ has factorized support: $\mathcal{S}(\bar{q}_\theta(\mathbf{z})) = \mathcal{S}^\times(\bar{q}_\theta(\mathbf{z}))$. While the factorized support in the definition implies independently sampling of \mathbf{z}^i , we theoretically and empirically show that mixing between two images and K images are equivalent (see Appendix A.2). We now illustrate how we derive a mixing strategy between two images based on the specific compositional structure of factors for attribute and object disentanglement.

Mixing Strategy for Attribute Disentanglement In attribute disentanglement, it is typically assumed that each scene is composed of K unique factors. For example, a human face consists of fixed set of features such as eyes, a nose, a mouth, and ears, with each factor being distinctive and included only once. It indicates that our mixing strategy should guarantee mutual exclusiveness in mixing $\mathbf{z}^1, \mathbf{z}^2$ to ensure the resulting \mathbf{z}^c always contain K distinct factors. Based on this compositional structure for attribute disentanglement, we design a corresponding mixing strategy between two images $\mathbf{x}^1, \mathbf{x}^2$ by randomly selecting each latent \mathbf{z}_i exclusively from either \mathbf{z}_i^1 or \mathbf{z}_i^2 (see Figure 1 (a) above), *i.e.*, each latent \mathbf{z}_i is drawn from one of the two, but never from both.

Specifically, let I^S be a randomly sampled subset of the index set $I = \{1, \dots, K\}$. The mixing strategy π_{attr} for attribute disentanglement is defined as:

$$\pi_{attr}(\mathbf{z}^1, \mathbf{z}^2) = \{\mathbf{z}_j^1 | j \in I^S\} \cup \{\mathbf{z}_j^2 | j \in I - I^S\} \quad (2)$$

Our mixing strategy (Equation 2) shares connection to random permutation trick in FactorVAE (Kim & Mnih, 2018). FactorVAE explicitly forms a factorized posterior by randomly mixing each dimension of the latent representations among different images. However, FactorVAE assumes statistical independence on the latent space and propose to minimize KL divergence between a factorized posterior (*i.e.*, distribution of randomly mixed samples) and a aggregated posterior (distribution of sample). Such objective is specifically tailored for statistical independent factors of variation, make it trivial to apply this objective into disentangling other class of factors of variation, *e.g.*, object. In contrast, we implement our inductive bias as a mixing strategy, we can without modifying the objective function, which will be introduced in next paragraph.

Mixing Strategy for Object Disentanglement Object-centric learning often assumes that a scene is composed of a set of objects, where all objects are regarded as same class of factors of variation (Greff

et al., 2019). For instance, as all objects belong to same class of factor, replacing an object in image with any object from different images remain realistic. Therefore, each disentangled representation \mathbf{z}_i can encode any object, indicating that all \mathbf{z}_i share the same support set, *i.e.*, $\mathcal{S}(p(\mathbf{z}_i)) = \mathcal{S}(p(\mathbf{z}_j))$ for $i, j \in \{1, \dots, K\}$. Since all \mathbf{z}_i share the same support, for disentangled representation, it satisfies $\mathcal{S}(p(\mathbf{z})) = \mathcal{S}(p(\mathbf{z}_1)) \times \dots \times \mathcal{S}(p(\mathbf{z}_K)) = \mathcal{S}(p(\mathbf{z}_{r_1})) \times \dots \times \mathcal{S}(p(\mathbf{z}_{r_K}))$, where $r_i \in \{1, \dots, K\}$ in definition 1. It indicates that there must exist \mathbf{z} from some image \mathbf{x} for any arbitrary combinations of object representations without considering mutual exclusiveness as in mixing for attributes. This necessitates a mixing strategy that accommodates arbitrary object combinations, enabling the replacement of any \mathbf{z}_i with any \mathbf{z}_j . Accordingly, the mixing strategy for object disentanglement involves randomly sampling K elements from the joint set $\mathbf{z}^1 \cup \mathbf{z}^2 \in \mathbb{R}^{2K \times D}$. Unlike the mixing strategy for attributes, this approach permits random exchanges between \mathbf{z}_i^1 and \mathbf{z}_j^2 between different indices (see Figure 1 below). Specifically, denoting I^{S_n} as a randomly sampled subset of the index set $I = \{1, \dots, K\}$ with cardinality n , *i.e.*, $\{I^S | I^S \subseteq I, |I^S| = n\}$. Then the corresponding mixing strategy π_{obj} for object disentanglement is defined as:

$$\pi_{obj}(\mathbf{z}^1, \mathbf{z}^2) = \{\mathbf{z}_j^1 | j \in I^{S_n}\} \cup \{\mathbf{z}_j^2 | j \in I^{S_{K-n}}\}, n \sim U(0, K) \quad (3)$$

3.3 LEARNING OBJECTIVES

In this section, we illustrate the overall learning objectives to instantiate our framework. Following the recent approaches, our framework is built upon the auto-encoding framework. Specifically, instead of directly reconstructing the image, we minimize a denoising objective using a diffusion decoder, following state-of-the-art methods (Yang et al., 2023; Jung et al., 2024) for both attribute and object disentanglement, as:

$$\mathcal{L}_{\text{Diff}}(\theta, \phi) = \mathbb{E}_{\epsilon \sim \mathcal{N}(\mathbf{0}, \mathbf{I}), t \sim U(0, 1)} [w(t) \cdot \|D_\phi(\mathbf{x}_t, t, E_\theta(\mathbf{x})) - \epsilon\|^2], \quad (4)$$

where $\mathbf{x}_t = \sqrt{\bar{\alpha}_t} \mathbf{x} + \sqrt{1 - \bar{\alpha}_t} \epsilon$ is a noised image of \mathbf{x} with timestep t , $\bar{\alpha}_t = \prod_{i=1}^t (1 - \beta_i)$ is a schedule function, and $w(t)$ is the weighting parameter. As we use diffusion decoder D_ϕ , we use iterative decoding when generating composite image \mathbf{x}^c from the diffusion decoder but omit the expression for notational simplicity. In addition to the auto-encoding objective, we employ two additional objectives: likelihood maximization objective and compositional consistency objective.

Maximizing Likelihood of Composite Images Given \mathbf{x}^c composed by our mixing strategy, we maximize the likelihood of \mathbf{x}^c . To maximize the likelihood of the composite image \mathbf{x}^c , we leverage a pre-trained diffusion model G_ψ for its reliable likelihood estimations and robust generative performance. Since the denoising loss in diffusion models serves as an upper bound for the negative log-likelihood Ho et al. (2020), minimizing the denoising loss with respect to \mathbf{x}^c effectively increases the likelihood $p(\mathbf{x}^c)$. However, due to the expensive and noisy computation of gradients in back-propagating through a large diffusion model, we follow (Poole et al., 2022; Jung et al., 2024) and apply an approximated gradient to optimize $p(\mathbf{x}^c)$:

$$\nabla_\theta \mathcal{L}_{\text{Prior}}(\theta) = \mathbb{E}_{t, \epsilon} [w(t) (G_\psi(\mathbf{x}_t^c, t) - \epsilon) \frac{\partial \mathbf{x}^c}{\partial \theta}], \quad (5)$$

where $t \sim \mathcal{U}(t_{\min}, t_{\max})$ is a timestep, $w(t)$ is a timestep-dependent function, $\epsilon \sim \mathcal{N}(\mathbf{0}, \mathbf{I})$ is a Gaussian noise. $\mathbf{x}_t^c = \sqrt{\bar{\alpha}_t} \mathbf{x}^c + \sigma_t \epsilon$ denotes a noised image of \mathbf{x}^c with the forward diffusion process.

While Jung et al. (2024) also maximizes the compositionality of object-representations with the generative prior, the authors propose reusing D_ϕ —the diffusion decoder jointly trained with the encoder in Equation 4—for G_ψ , optimizing $\nabla_\theta \mathcal{L}'_{\text{Prior}}(\theta) = \mathbb{E}_{t, \epsilon} [w(t) (D_\phi(\mathbf{x}_t^c, t, \mathbf{z}^c) - \epsilon) \frac{\partial \mathbf{x}^c}{\partial \theta}]$ instead of Equation 5. We argue that diffusion decoder D_ϕ is in fact estimates $p(\mathbf{x}^c | \mathbf{z}^c)$ rather than $p(\mathbf{x}^c)$, making them unsuitable for estimating $p(\mathbf{x}^c)$. Thus, we instead opt for a separately pre-trained unconditional diffusion model for G_ψ .

Compositional Consistency Loss In addition to maximizing the likelihood $p(\mathbf{x}^c)$, we encourage computational consistency between \mathbf{z}^c and $\hat{\mathbf{z}}^c = E_\theta(D_\phi(\mathbf{z}^c))$ to avoid generating realistic images regardless of the given \mathbf{z}^c . A straightforward way to promote compositional consistency is to minimize the cosine distance between \mathbf{z}^c and the inverted latent $\hat{\mathbf{z}}^c = E_\theta(D_\phi(\mathbf{z}^c))$. However, our empirical observations reveal that even with this direct minimization, the resulting \mathbf{x}^c can remain

irrelevant to \mathbf{z}^c . This occurs because the encoder can collapse the posterior $p_\theta(\mathbf{z}|\mathbf{x})$ into a single mode¹, causing any two latents encoded by the encoder to maintain a small distance. In such cases, the decoder generating random realistic images for \mathbf{z}^c may produce a small distance between the original and inverted latents, regardless of consistency. To address this issue, we instead minimize the *relative* distance between \mathbf{z}^c and $\hat{\mathbf{z}}^c$, *i.e.*, the distance relative to negative samples, which are latents from other random images. This prevents the encoder from collapsing the posterior into a single mode, as \mathbf{z}^c must not only match $\hat{\mathbf{z}}^c$ but also be distinguished from negative samples. Formally, we define the compositional consistency loss is defined as:

$$\mathcal{L}_{\text{Con}}(\theta) = -\log \frac{\exp(d(\hat{\mathbf{z}}^c, \mathbf{z}^c)/\tau)}{\sum_{i \in \{1, \dots, B\}} \exp(d(\hat{\mathbf{z}}^c, \mathbf{z}^i)/\tau)}, \quad (6)$$

where τ and $d(\cdot)$ denote temperature and cosine similarity, respectively, and B is a batch size. Note that we should consider the correspondence between $\mathbf{z}^c = \{\mathbf{z}_1^c, \dots, \mathbf{z}_K^c\}$ and $\hat{\mathbf{z}}^c = \{\hat{\mathbf{z}}_1^c, \dots, \hat{\mathbf{z}}_K^c\}$ to compute the cosine distance. This can be problematic for object disentanglement, as object-disentangled representations can have permuted orders due to our mixing strategy. In this case, we first apply the Sinkhorn-Knopp algorithm (Cuturi, 2013) to compute a soft assignment between \mathbf{z}^c and $\hat{\mathbf{z}}^c$, then use the assignment-weighted sum of the distances to compute the loss.

Overall Objectives In summary, our framework is built upon an auto-encoding framework, which is implemented with denoising objective. To maximize the compositionality of composite images, we maximize the likelihood of the composite image \mathbf{x}^c with pre-trained diffusion model G_ψ , and enforce compositional consistency to ensure resulting \mathbf{x}^c consistent to \mathbf{z}^c . The overall objective is given as:

$$\mathcal{L}_{\text{Total}}(\theta, \phi) = \mathcal{L}_{\text{Diff}}(\theta, \phi) + \lambda_{\text{Prior}} \mathcal{L}_{\text{Prior}}(\theta) + \lambda_{\text{Con}} \mathcal{L}_{\text{Con}}(\theta), \quad (7)$$

where λ_{Prior} and λ_{Con} controls the relative importance of the objectives. Note that these objectives are not tailored specific to each factors of variation, but instead shared for both attribute and object disentanglement.

4 EXPERIMENT

Implementation Details We use the same encoder and decoder architectures as the baselines (Yang et al., 2023; Jung et al., 2024) for a fair comparison. Following the state-of-the-art methods in attribute (Yang et al., 2023) and object (Jiang et al., 2023) disentanglements, we employ a pre-trained VAE (Rombach et al., 2022) to represent an image as a latent feature and a latent diffusion model (Rombach et al., 2022) for the decoder D_ϕ . Since the diffusion decoder operates on VAE features, we adjust our image encoder to take VAE features as an input. When generating the image \mathbf{x}^c from \mathbf{z}^c , we iteratively decode images using only a few steps (1 to 4 steps) following DDIM (Song et al., 2020) to efficiently reduce the costly iterative decoding process. When back-propagate the gradient through \mathbf{x}^c , we truncate the gradient at the last iteration of decoding. Also, to ensure the reliable image generation from few-step decoding, we use a v-prediction objective when training the diffusion model (Salimans & Ho, 2022). For the generative prior G_ψ , we train an unconditional diffusion model on each training dataset from the scratch. More implementation details can be found in the Appendix A.4.

4.1 ATTRIBUTE DISENTANGLEMENT

Datasets We evaluate our method on three standard datasets in disentangled representation learning. Shapes3D (Kim & Mnih, 2018) consists of 3D shapes with 6 ground truth factors. Cars3D (Reed et al., 2015) is a dataset of 3D car models with 3 ground truth factors. MPI3D (Gondal et al., 2019) contains physical 3D objects with 7 factors of variation. All experiments are conducted at a 64x64 image resolution, following (Ren et al., 2022; Yang et al., 2023).

Evaluation Metrics We use two evaluation metrics: the FactorVAE (Kim & Mnih, 2018) score and the DCI (Eastwood & Williams, 2018) metric. The FactorVAE score measures disentanglement

¹ We measured the pairwise cosine distances between latents from different images and observed that all of them are significantly low

Table 1: Comparisons of attribute disentanglement on the FactorVAE score and DCI disentanglement metrics. Our method achieves state-of-the-art performance in almost all of the datasets, except FactorVAE score in Cars3D.

Method	Cars3D		Shapes3D		MPI3D	
	FactorVAE	DCI	FactorVAE	DCI	FactorVAE	DCI
FactorVAE (Kim & Mnih, 2018)	0.906±0.052	0.161±0.019	0.840±0.066	0.611±0.082	0.152±0.025	0.240±0.051
β -TCVAE (Chen et al., 2018)	0.855±0.082	0.140±0.019	0.873±0.074	0.613±0.114	0.179±0.017	0.237±0.056
InfoGAN-CR (Lin et al., 2020b)	0.411±0.013	0.020±0.011	0.587±0.058	0.478±0.055	0.439±0.061	0.241±0.056
LD (Voynov & Babenko, 2020)	0.852±0.039	0.216±0.072	0.805±0.064	0.380±0.064	0.391±0.039	0.196±0.038
GS (Härkönen et al., 2020)	0.932±0.018	0.209±0.031	0.788±0.091	0.284±0.034	0.464±0.036	0.229±0.042
DisCo (Ren et al., 2022)	0.855±0.074	0.271±0.037	0.877±0.031	0.708±0.048	0.371±0.030	0.292±0.024
DisDiff-VQ (Yang et al., 2023)	0.976±0.018	0.232±0.019	0.902±0.043	0.723±0.013	0.617±0.070	0.337±0.057
Ours	0.877±0.089	0.365±0.073	0.975±0.059	0.837±0.105	0.668±0.055	0.409±0.035

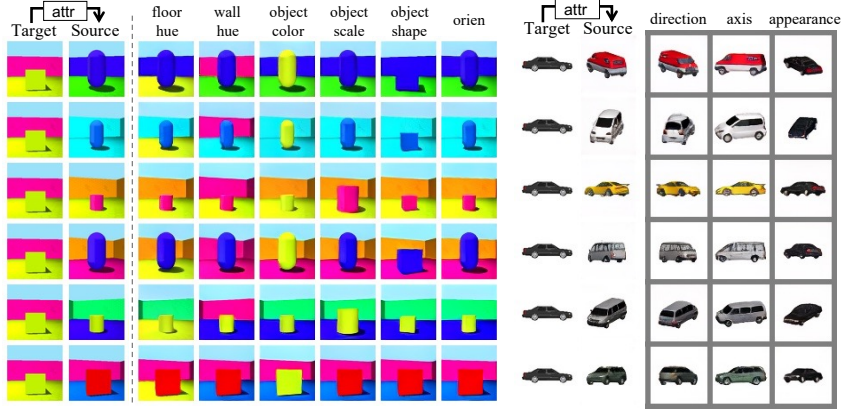


Figure 2: Qualitative results on Shapes3D and Cars3D. We swap each latent of source image with the one in target image. Our model successfully identifies six underlying factors in shape3D. In Cars3D, our method discovered three factors including appearance, direction, axis.

using majority vote classifiers trained to predict the changing ground-truth factor. The DCI metric quantifies disentanglement by assessing each dimension’s dominance in predicting each attribute. Since our method induces a vector-wise disentanglement, we perform PCA as post-processing on the representation before evaluation, following (Du et al., 2021; Yang et al., 2023).

Baselines We compare our method with state-of-the-art baselines: (1) VAE-based methods, including FactorVAE Kim & Mnih (2018) and β -TCVAE Chen et al. (2018), (2) GAN-based methods, including InfoGAN-CR Lin et al. (2020b), GANspace (GS) Härkönen et al. (2020), LatentDiscovery (LD) Voynov & Babenko (2020), and DisCo Ren et al. (2022), and (3) the diffusion-based model DisDiff Yang et al. (2023). We mostly follow the experimental settings in DisDiff and use the same encoder and diffusion decoder architecture as DisDiff.

Main Results We first report the comparison results of our method with baselines for attribute disentanglement in Table 1. Our method outperforms all baselines on the Shapes3D and MPI3D datasets by a clear margin, achieving 8% higher FactorVAE scores and 15.7% to 21.4% higher DCI metrics compared to the second-best baselines. For the Cars3D dataset, our method achieves the best DCI metric. Notably, on Shapes3D and MPI3D datasets, our method outperforms the state-of-the-art baseline DisDiff (Yang et al., 2023) with substantial margin. This indicates the effectiveness of our objective in directly enforcing the support factorization between latent representations via our mixing strategy for disentangling factors, compared to using an approximate measure such as the upper bound of mutual information between latents.

Note that our method also significantly outperforms FactorVAE (Kim & Mnih, 2018), which similarly utilizes random mixing of representations. We hypothesize that our method benefits from flexible choice of model architectures. Specifically, FactorVAE is specifically designed to disentangle between latent dimensions within VAE framework to explicitly minimize Total Correlation. In

contrast, our framework can freely choose the model architecture, so our model benefits from vector-wise disentanglement and expressive decoder, *i.e.*, diffusion model, which are known to have better disentanglement and representation quality. Overall, the quantitative results demonstrate the effectiveness of our model in attribute disentanglement.

To further analyze the quality of our disentangled representations, we perform image generation by swapping the latent representations between images in Fig. 2. We first encode a randomly sampled target image and six randomly sampled source images into K latent representations each. For each $k \in \{1, \dots, K\}$, we then construct swapped representations by replacing the k th latent representation from the target image with the k th latent representation from the source images and decode these swapped representations. The results demonstrate the effectiveness of our method in attribute disentanglement and compositional image generation. Surprisingly, in the Shapes3D dataset, our method successfully identifies all six ground-truth factors of variation. In the Cars3D dataset, our method captures three independent factors, enabling controlled manipulation of each factor.

4.2 OBJECT DISENTANGLEMENT

Datasets We evaluate our method for object disentanglement on three multi-object datasets. CLEVR-Easy (Singh et al., 2022b) contains images with 2-3 objects in different colors, shapes, and positions. CLEVR (Johnson et al., 2017) consists of images containing 3-10 objects, further differing in size and material compared to CLEVR-Easy. In CLEVR-Tex (Singh et al., 2022b), textures are added to objects and backgrounds of the CLEVR dataset, leading more complex scenes with diverse materials. All images in the datasets are center-cropped and resized to 128×128 pixels.

Evaluation Protocol We evaluate the quality of object representations through an object property prediction task, following (Jiang et al., 2023; Jung et al., 2024). For each property, we train a network to predict the property based on frozen object representations. Correspondences between the each representation and GT objects are determined through Hungarian matching using masks. For baselines, slot-attention masks are used for matching. In contrast, as our method does not produce masks, we identify the corresponding region of the object representation by averaging the differences in output images when we compose each representation with other representations. For the classifier, we employ a 2-layer MLP with a hidden dimension of 256. We report accuracy for categorical properties and mean squared error (MSE) for continuous properties.

Baselines We compare our method with object-centric learning methods leveraging slot-attention: SA (Locatello et al., 2020) and SLASH (Kim et al., 2023). Also, we compare our method against state-of-the-art methods using the diffusion decoders: LSD (Jiang et al., 2023) and L2C (Jung et al., 2024). It’s worth noting that ours does not employ slot attention or any kinds of spatial-exclusiveness biases. For a fair comparison, we employ the same encoder architecture across all baselines including ours, and all diffusion-based methods share the same decoder.

Main Results Tab. 2 presents the results of the object property prediction task. Our method achieves competitive performance compared to state-of-the-art baselines, LSD (Jiang et al., 2023) and L2C (Jung et al., 2024), demonstrating its effectiveness in object-centric learning. Notably, our method outperforms LSD on CLEVR-Tex and achieves comparable performance on CLEVR and CLEVR-Easy. Considering the primary difference between LSD and our method is the use of slot attention versus the compositionality maximization by mixing strategy, our method’s competitive performance validates the effectiveness of our mixing strategy as a strong inductive bias for object disentanglement. In comparison to L2C, our method achieves better performance on CLEVR and CLEVR-Easy while being competitive on CLEVR-Tex. In CLEVR dataset, we observed that slot attention in L2C got undesirable positional biases. Since L2C maximizes conditional likelihood $p(\mathbf{x}^c | \mathbf{z}^c)$, it can be achieved by local encoding and decoding instead of maximizing $p(\mathbf{x})$. Overall, the competitive performance of our method compared to strong baselines verifies that our mixing strategy provides robust inductive bias for object-centric learning.

We further explore the compositionality of our latent representations in Fig. 3. Given pairs of images, we encode each image into K object representations and construct a mixed representation by randomly exchanging one latent between images. The mixed representations are then decoded with the decoder to produce final composite images. In Fig. 3, we replace one object (depicted with red

Table 2: Comparison of object disentanglement on property prediction. For the position* property of CLEVEasy dataset, we use the discrete labels provided in the dataset and reports the accuracy.

Method	CLEVEasy			CLEVR				CLEVRTex		
	Shape (↑)	Color (↑)	Position* (↑)	Shape (↑)	Color (↑)	Material (↑)	Position (↓)	Shape (↑)	Material (↑)	Position (↓)
SA	72.25	72.33	44.08	79.4	91.30	93.18	0.064	30.44	7.890	0.482
SLASH	86.06	89.23	46.97	83.28	<u>92.26</u>	93.16	0.078	53.13	37.49	0.148
LSD	96.03	98.05	<u>50.29</u>	87.66	91.46	94.87	<u>0.062</u>	68.25	51.54	0.197
L2C	92.78	93.57	47.62	73.61	74.03	86.93	0.168	71.54	<u>51.62</u>	0.116
Ours	<u>95.81</u>	<u>95.38</u>	50.72	<u>87.04</u>	93.93	<u>94.81</u>	0.032	<u>70.90</u>	52.2	<u>0.133</u>

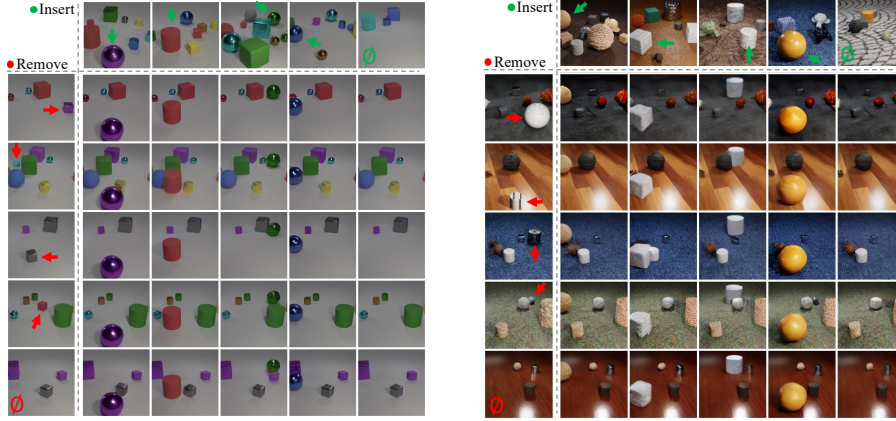


Figure 3: Qualitative results on object-wise manipulation in CLEVR and CLEVRTex. Objects depicted with red arrows are replaced by the one depicted with green arrows. Successful object-wise manipulation verifies that our method successfully disentangles the objects. We also find *empty* latent (depicted with ϕ), which makes our approach capable of handling varying number of objects.

arrow) from first column with the object (depicted with red arrow) from first row’s image. In second to fifth column, we identify successful insertion of the individual objects depicted in to first row into the first column’s image. Meanwhile, the objects depicted with red arrows are successfully removed from the original scene. It demonstrates that our method successfully disentangle individual objects. Notably, in fifth row and fifth column, we observe that our method allows the emergence of latent encoding empty information. When manipulate such latent, it does not add any of the objects (in fifth column) or remove none of the objects (in fifth row) from the original images. It highlights that our method is capable of capturing varying number of objects.

4.3 ABLATION STUDY

Impact of Losses We conduct an ablation study on the impact of each term in our objectives and present the results in Tab. 3. The results indicate that incorporating all three losses of diffusion ($\mathcal{L}_{\text{Diff}}$), prior ($\mathcal{L}_{\text{Prior}}$), and cycle loss (\mathcal{L}_{Con}) is essential for our method. In attribute disentanglement learning, sequentially adding each loss term consistently improves performance, with the best results achieved when all losses are combined. In contrast, for object disentanglement learning, clear performance gains across all three property predictions are observed only when using all loss terms together, possibly due to differences in the mixing strategy.

Impact of Mixing Strategy We investigate the importance of an appropriate mixing strategy for attribute and object disentanglement learning. We experimented with object mixing and attribute mixing applied interchangeably to attribute disentanglement learning and object disentanglement learning, respectively. The results are shown in the bottom three rows of Tab. 3. The results show that the interchanged mixing strategy significantly degrades performance, in both attribute and object disentanglement learning, highlighting the importance of a proper mixing strategy in our method.

Table 3: Ablation study on our method. We investigate the impact of each learning objective and mixing strategy. It confirms that our method work best with all of the objectives and proper choice of mixing strategy improves disentanglement.

		Shape3D		Clevr		
		FactorVAE	DCI	Shape (\uparrow)	Color (\uparrow)	Position (\downarrow)
Impact of Losses	$\mathcal{L}_{\text{Diff}}$	0.492	0.175	62.270	88.580	0.111
	$\mathcal{L}_{\text{Diff}} + \mathcal{L}_{\text{Prior}}$	0.597	0.224	63.393	86.943	0.126
	$\mathcal{L}_{\text{Diff}} + \mathcal{L}_{\text{Cycle}}$	0.769	0.597	64.210	80.279	0.116
	$\mathcal{L}_{\text{Diff}} + \mathcal{L}_{\text{Prior}} + \mathcal{L}_{\text{Cycle}}$	1.000	0.887	87.039	93.928	0.032
Impact of Mixing Strategy	Attribute mixing	1.000	0.887	65.236	80.520	0.119
	Object mixing	0.634	0.127	87.040	93.928	0.033

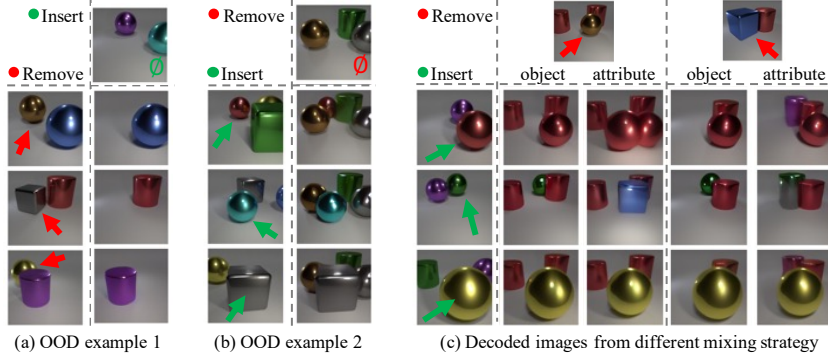


Figure 4: Qualitative analysis on our method. Our analysis verifies that our method can generalize to out-of-distribution (OOD) scenes (a), (b) and highlights the importance of choosing an appropriate mixing strategy (c).

More qualitative analysis In Fig 4-(a, b), we observe that our method is capable of generating out-of-distribution (OOD) examples that do not exist in the dataset, but can be created through composition. Notably, using the CLEVR-Easy dataset, which comprises images with 2-3 objects, our method can generate high-quality images containing either a single object or 4 objects through composition, by inserting or removing the representation that does not encodes object. In Fig 4-(c), we compare images composed from models trained using different mixing strategies: object mixing and attribute mixing. As demonstrated in the main results and our ablation study, the object mixing strategy allows for object-level manipulation. In contrast, while the attributed mixing strategy, also supported by the prior loss, produces images of reasonable quality, but it does not achieve object-level modifications. Specifically, when object slots are swapped, the changes in the image are not confined to a single object but also alter the properties of other objects.

5 LIMITATIONS AND FUTURE WORK

While our method aims to identify underlying factors of variations by compositionality within the representation, discovered factor may not exactly aligned to ground-truth factors. As data may not be decomposed in a unique way, it's challenging to discover the exact decomposition of data using our method. In this work, our framework demonstrates how to uncover the general factors of variation, focusing on the representative examples in the field (e.g., attributes and objects.). For future work, we will further explore nuanced and intricate factors of variation within the data.

6 CONCLUSION

In this paper, we introduced a unified framework for disentangled representation learning that is compatible with both attribute and object disentanglement. We formulate disentangled representation learning as the process of maximizing compositionality within the representation, enabling both attribute and object disentanglement by controlling only the composition operator. Although compatible with both attribute and object disentanglement, our method achieved competitive performance against strong baselines in each domain.

REFERENCES

- Yoshua Bengio and Yann LeCun. Scaling learning algorithms toward ai. 2007.
- Christopher P Burgess, Irina Higgins, Arka Pal, Loic Matthey, Nick Watters, Guillaume Desjardins, and Alexander Lerchner. Understanding disentangling in β -vae. In *ICLR*, 2017.
- Christopher P Burgess, Loic Matthey, Nicholas Watters, Rishabh Kabra, Irina Higgins, Matt Botvinick, and Alexander Lerchner. Monet: Unsupervised scene decomposition and representation. *arXiv preprint arXiv:1901.11390*, 2019.
- Ricky TQ Chen, Xuechen Li, Roger B Grosse, and David K Duvenaud. Isolating sources of disentanglement in variational autoencoders. *Advances in neural information processing systems*, 31, 2018.
- Xi Chen, Yan Duan, Rein Houthooft, John Schulman, Ilya Sutskever, and Pieter Abbeel. Info-gan: Interpretable representation learning by information maximizing generative adversarial nets. *Advances in neural information processing systems*, 29, 2016.
- Marco Cuturi. Sinkhorn distances: Lightspeed computation of optimal transport. *Advances in neural information processing systems*, 26, 2013.
- Yilun Du, Shuang Li, Yash Sharma, Josh Tenenbaum, and Igor Mordatch. Unsupervised learning of compositional energy concepts. *Advances in Neural Information Processing Systems*, 34: 15608–15620, 2021.
- Cian Eastwood and Christopher KI Williams. A framework for the quantitative evaluation of disentangled representations. In *International conference on learning representations*, 2018.
- Martin Engelcke, Adam R Kosior, Oivi Parker Jones, and Ingmar Posner. Genesis: Generative scene inference and sampling with object-centric latent representations. In *ICLR*, 2020.
- Muhammad Waleed Gondal, Manuel Wuthrich, Djordje Miladinovic, Francesco Locatello, Martin Breidt, Valentin Volchkov, Joel Akpo, Olivier Bachem, Bernhard Schölkopf, and Stefan Bauer. On the transfer of inductive bias from simulation to the real world: a new disentanglement dataset. *Advances in Neural Information Processing Systems*, 32, 2019.
- Ian Goodfellow, Jean Pouget-Abadie, Mehdi Mirza, Bing Xu, David Warde-Farley, Sherjil Ozair, Aaron Courville, and Yoshua Bengio. Generative adversarial networks. *Communications of the ACM*, 63(11):139–144, 2020.
- Klaus Greff, Raphaël Lopez Kaufman, Rishabh Kabra, Nick Watters, Christopher Burgess, Daniel Zoran, Loic Matthey, Matthew Botvinick, and Alexander Lerchner. Multi-object representation learning with iterative variational inference. In *ICML*, 2019.
- Erik Härkönen, Aaron Hertzmann, Jaakko Lehtinen, and Sylvain Paris. Ganspace: Discovering interpretable gan controls. *Advances in neural information processing systems*, 33:9841–9850, 2020.
- Irina Higgins, David Amos, David Pfau, Sebastien Racaniere, Loic Matthey, Danilo Rezende, and Alexander Lerchner. Towards a definition of disentangled representations. *arXiv preprint arXiv:1812.02230*, 2018.
- Jonathan Ho, Ajay Jain, and Pieter Abbeel. Denoising diffusion probabilistic models. In *NeurIPS*, 2020.
- Jindong Jiang, Fei Deng, Gautam Singh, and Sungjin Ahn. Object-centric slot diffusion. In *NeurIPS*, 2023.
- Justin Johnson, Bharath Hariharan, Laurens Van Der Maaten, Li Fei-Fei, C Lawrence Zitnick, and Ross Girshick. Clevr: A diagnostic dataset for compositional language and elementary visual reasoning. In *Proceedings of the IEEE conference on computer vision and pattern recognition*, pp. 2901–2910, 2017.

- Whie Jung, Jaehoon Yoo, Jaehoon Ahn, and Jaehoon Hong. Learning to compose: Improving object centric learning by injecting compositionality. In *ICLR*, 2024.
- Hyunjik Kim and Andriy Mnih. Disentangling by factorising. In *International conference on machine learning*, pp. 2649–2658. PMLR, 2018.
- Jinwoo Kim, Janghyuk Choi, Ho-Jin Choi, and Seon Joo Kim. Shepherding slots to objects: Towards stable and robust object-centric learning. In *CVPR*, 2023.
- Yen-Ling Kuo, Boris Katz, and Andrei Barbu. Compositional networks enable systematic generalization for grounded language understanding. In *EMNLP*, 2021.
- Brenden M Lake, Tomer D Ullman, Joshua B Tenenbaum, and Samuel J Gershman. Building machines that learn and think like people. *Behavioral and brain sciences*, 40:e253, 2017.
- Junnan Li, Dongxu Li, Silvio Savarese, and Steven Hoi. BLIP-2: Bootstrapping language-image pre-training with frozen image encoders and large language models. In Andreas Krause, Emma Brunskill, Kyunghyun Cho, Barbara Engelhardt, Sivan Sabato, and Jonathan Scarlett (eds.), *Proceedings of the 40th International Conference on Machine Learning*, volume 202 of *Proceedings of Machine Learning Research*, pp. 19730–19742. PMLR, 23–29 Jul 2023. URL <https://proceedings.mlr.press/v202/li23q.html>.
- Zhixuan Lin, Yi-Fu Wu, Skand Vishwanath Peri, Weihao Sun, Gautam Singh, Fei Deng, Jindong Jiang, and Sungjin Ahn. Space: Unsupervised object-oriented scene representation via spatial attention and decomposition. In *ICLR*, 2020a.
- Zinan Lin, Kiran Thekumparampil, Giulia Fanti, and Sewoong Oh. Infogan-cr and modelcentrality: Self-supervised model training and selection for disentangling gans. In *international conference on machine learning*, pp. 6127–6139. PMLR, 2020b.
- Francesco Locatello, Stefan Bauer, Mario Lucic, Gunnar Raetsch, Sylvain Gelly, Bernhard Schölkopf, and Olivier Bachem. Challenging common assumptions in the unsupervised learning of disentangled representations. In *international conference on machine learning*, pp. 4114–4124. PMLR, 2019.
- Francesco Locatello, Dirk Weissenborn, Thomas Unterthiner, Aravindh Mahendran, Georg Heigold, Jakob Uszkoreit, Alexey Dosovitskiy, and Thomas Kipf. Object-centric learning with slot attention. In *NeurIPS*, 2020.
- Aaron van den Oord, Yazhe Li, and Oriol Vinyals. Representation learning with contrastive predictive coding. *arXiv preprint arXiv:1807.03748*, 2018.
- Ben Poole, Ajay Jain, Jonathan T Barron, and Ben Mildenhall. Dreamfusion: Text-to-3d using 2d diffusion. In *ICLR*, 2022.
- Scott E Reed, Yi Zhang, Yuting Zhang, and Honglak Lee. Deep visual analogy-making. *Advances in neural information processing systems*, 28, 2015.
- Xuanchi Ren, Tao Yang, Yuwang Wang, and Wenjun Zeng. Learning disentangled representation by exploiting pretrained generative models: A contrastive learning view. In *ICLR*, 2022.
- Robin Rombach, Andreas Blattmann, Dominik Lorenz, Patrick Esser, and Björn Ommer. High-resolution image synthesis with latent diffusion models. In *CVPR*, pp. 10684–10695, 2022.
- Karsten Roth, Mark Ibrahim, Zeynep Akata, Pascal Vincent, and Diane Bouchacourt. Disentanglement of correlated factors via hausdorff factorized support. In *ICLR*, 2023.
- Tim Salimans and Jonathan Ho. Progressive distillation for fast sampling of diffusion models. *arXiv preprint arXiv:2202.00512*, 2022.
- Gautam Singh, Fei Deng, and Sungjin Ahn. Illiterate dall-e learns to compose. In *ICLR*, 2022a.
- Gautam Singh, Yeongbin Kim, and Sungjin Ahn. Neural systematic binder. In *The Eleventh International Conference on Learning Representations*, 2022b.

- Jiaming Song, Chenlin Meng, and Stefano Ermon. Denoising diffusion implicit models. *arXiv preprint arXiv:2010.02502*, 2020.
- Andrey Voynov and Artem Babenko. Unsupervised discovery of interpretable directions in the gan latent space. In *International conference on machine learning*, pp. 9786–9796. PMLR, 2020.
- Satosi Watanabe. Information theoretical analysis of multivariate correlation. *IBM Journal of research and development*, 4(1):66–82, 1960.
- Ziyi Wu, Jingyu Hu, Wuyue Lu, Igor Gilitschenski, and Animesh Garg. Slotdiffusion: Object-centric generative modeling with diffusion models. *Advances in Neural Information Processing Systems*, 36:50932–50958, 2023.
- Tao Yang, Yuwang Wang, Yan Lu, and Nanning Zheng. Disdiff: Unsupervised disentanglement of diffusion probabilistic models. *NeurIPS*, 2023.

A APPENDIX

A.1 RELATED WORK

Disentangled Representation Learning Disentangled representation learning for attribute disentanglement heavily rely on regularization terms in learning objectives (Burgess et al., 2017; Chen et al., 2016; Kim & Mnih, 2018; Chen et al., 2018; Ren et al., 2022; Yang et al., 2023). VAE-based models (Burgess et al., 2017; Kim & Mnih, 2018; Chen et al., 2018) demonstrates that controlling the importance of total correlation between latent dimensions hidden in the ELBO bounds encourages to disentangle independent factors. Empowered with enhanced generative models such as GANs (Goodfellow et al., 2020) and diffusion models (Ho et al., 2020), (Chen et al., 2016; Lin et al., 2020b) optimizes the mutual information between latents and generated images by GANs, and (Ren et al., 2022; Yang et al., 2023) proposed to optimize contrastive loss (Oord et al., 2018) or mutual information between the latents using pretrained GANs and diffusion model, respectively. Such information-theoretic approaches have shown promising disentangling capabilities, but it becomes challenging when a scene does not consist of fixed combination of factors, especially when there exists repeated appearances of the same factors, as seen in object-centric scenes.

Object-Centric Learning Built on the observation that each pixel in a scene must correspond exclusively to an unique object, the spatial-exclusive mechanism has been recognized as a key inductive bias in object-centric learning (Burgess et al., 2019; Greff et al., 2019; Engelcke et al., 2020; Locatello et al., 2020; Kim et al., 2023; Singh et al., 2022a). Early attempts in object-centric learning employed spatial masks to compose independently decoded RGB images from each latent (Burgess et al., 2019; Greff et al., 2019; Lin et al., 2020a; Engelcke et al., 2020). In addition to the spatial-exclusive bias, iterative refinement of each latent representation gradually improves the initially inaccurate spatial association between each latent and the pixels of the image (Greff et al., 2019). In slot attention (Locatello et al., 2020), each latent (slot), is randomly initialized and iteratively refined by a dot-product attention mechanism normalized over the slots. This mechanism induces competition between the slots to bind to spatial locations in the scene. Empowered by strong generative models combined with Slot Attention, recent studies (Singh et al., 2022a; Jiang et al., 2023; Wu et al., 2023; Jung et al., 2024) have demonstrated remarkable performance in unsupervised object discovery on complex real-world datasets. While these architectural biases excel at object disentanglement, strong assumption on spatial exclusiveness limits their applicability to disentangling non-spatial exclusive factors, such as attributes.

A.2 PROOF ON EQUIVALENCE BETWEEN MIXING TWO AND MULTIPLE IMAGES.

In this section, we explain why the random mixing between two images (*i.e.*, $\mathbf{z}^c = \pi(\mathbf{z}^1, \mathbf{z}^2)$) can replace the random composition of \mathbf{z}_i from K images. Formally, we will show that:

$$\text{If } \mathcal{S}(p(\mathbf{z})) = \mathcal{S}(p(\mathbf{z}^c)) \quad \text{then} \quad \mathcal{S}(p(\mathbf{z})) = \mathcal{S}^\times(p(\mathbf{z})), \quad (8)$$

where the factorized support $\mathcal{S}^\times(p(\mathbf{z})) = \mathcal{S}(p(\mathbf{z}_1)) \times \mathcal{S}(p(\mathbf{z}_2)) \times \dots \times \mathcal{S}(p(\mathbf{z}_K))$ represents the random composition of each latent variable \mathbf{z}_i from K images.

Proof. Given $\mathcal{S}(p(\mathbf{z})) = \mathcal{S}(p(\mathbf{z}^c))$, we can prove the followings:

1. If $p(\mathbf{z}_1)p(\mathbf{z}_2) > 0$ then $p(\mathbf{z}_1, \mathbf{z}_2) > 0$.
Note that $p(\mathbf{z}_1) > 0$ and $p(\mathbf{z}_2) > 0$ ($\Leftrightarrow p(\mathbf{z}_1)p(\mathbf{z}_2) > 0$) indicates the existence of $\mathbf{z}^1, \mathbf{z}^2$ with $\mathbf{z}_1^1 = \mathbf{z}_1, \mathbf{z}_2^2 = \mathbf{z}_2$. By mixing \mathbf{z}^1 and \mathbf{z}^2 , we can compose \mathbf{z}^* where $\mathbf{z}_1^* = \mathbf{z}_1, \mathbf{z}_2^* = \mathbf{z}_2$. Then, by the definition of the support that $\mathcal{S}(p(\mathbf{z})) = \{\mathbf{z} | p(\mathbf{z}) > 0\}$ and the given condition $\mathbf{z}^* \in \mathcal{S}(p(\mathbf{z}^c)) = \mathcal{S}(p(\mathbf{z}))$, $p(\mathbf{z}_1, \mathbf{z}_2) \geq p(\mathbf{z}^*) > 0$.
2. Assume that for some $k \geq 2$, if $\prod_{i=1}^k p(\mathbf{z}_i) > 0 \rightarrow p(\mathbf{z}_1, \mathbf{z}_2, \dots, \mathbf{z}_k) > 0$ then $\prod_{i=1}^{k+1} p(\mathbf{z}_i) > 0 \rightarrow p(\mathbf{z}_1, \mathbf{z}_2, \dots, \mathbf{z}_k, \mathbf{z}_{k+1}) > 0$.
Note that $\prod_{i=1}^{k+1} p(\mathbf{z}_i) > 0$ implies $p(\mathbf{z}_{k+1}) > 0$ and $\prod_{i=1}^k p(\mathbf{z}_i) > 0$. By the given assumption, $p(\mathbf{z}_1, \mathbf{z}_2, \dots, \mathbf{z}_k) > 0$ and there exists $\mathbf{z}^1, \mathbf{z}^2$ where $\mathbf{z}_i^1 = \mathbf{z}_i$ for $i \in \{1, \dots, k\}$ and $\mathbf{z}_{k+1}^2 = \mathbf{z}_{k+1}$. By mixing \mathbf{z}^1 and \mathbf{z}^2 , we can compose \mathbf{z}^* where $\mathbf{z}_i^* = \mathbf{z}_i$ for $i \in \{1, \dots, k+1\}$. As a result, by the given condition $\mathbf{z}^* \in \mathcal{S}(p(\mathbf{z}^c)) = \mathcal{S}(p(\mathbf{z}))$, $p(\mathbf{z}_1, \mathbf{z}_2, \dots, \mathbf{z}_k, \mathbf{z}_{k+1}) \geq p(\mathbf{z}^*) > 0$.

# of samples for mixing	Factor VAE	DCI
2	0.975±0.040	0.837±0.105
64	0.966±0.032	0.802±0.088

Table 4: Effects of number of samples used in mixing strategy

3. By mathematical induction, we conclude that if $\prod_{i=1}^K p(\mathbf{z}_i) > 0$ then $p(\mathbf{z}) > 0$.

Note that (3) implies $\mathcal{S}(p(\mathbf{z})) = \mathcal{S}^\times(p(\mathbf{z}))$, since $\mathcal{S}^\times(p(\mathbf{z}))$ can be expressed as $\{\mathbf{z} | p(\mathbf{z}_i) > 0\}$. By using mathematical induction, we have proved that random mixing between two images can replace the random composition of multiple images to achieve disentanglement.

A.3 EMPIRICAL RESULTS DIFFERENCE BETWEEN MIXING TWO AND MULTIPLE IMAGES.

In addition to theoretic result, we provide empirical results on our mixing strategy between two and multiple images (we use 64 here) are equivalent. We conduct experiments on attribute disentanglement with three different seeds and report FactorVAE and DCI in Table ???. We identified there is no meaningful difference between mixing two or 64 images, which supports our theoretical result.

A.4 ADDITIONAL IMPLEMENTATION DETAILS

In this section, we provide additional implementation details. When we train our method, we fix batch size of 64 and learning rate of 0.0001 across all of the experiments. We use $\lambda_{Prior} = 1$ and $\lambda_{Cycle} = 0.01$ for all experiments except $\lambda_{Cycle} = 0.1$ for the experiments in MPI3D dataset. We fix number of latents $K = 10$ in attribute disentanglement experiment following the best configuration of DisDiff (Yang et al., 2023) and $K = 4, 11, 11$ for CLEVEasy, CLEVR, CLEVRText, respectively, for object disentanglement.

Table 12,7,8,14 summarizes the hyper-parameters of our encoder and decoder architectures used in the experiments. Following DisDiff (Yang et al., 2023) and LSD (Jiang et al., 2023), we employ pretrained vq-vae² and kl-regularized auto-encoder model³ in attribute disentanglement and object disentanglement, respectively. In attribute disentanglement experiment, the encoder maps the input \mathbf{x} into 1-dimensional vector $\mathbf{z} \in \mathbb{R}^{KD}$ and we uniformly divide it into K latents. In object disentanglement experiment, to support the mapping from varying number of inputs (e.g., different spatial resolutions of UNet feature) into K latent representations, we adopt QFormer (Li et al., 2023). Specifically, we have K learnable queries $\{\mathbf{q}\}^K \in \mathbb{R}^{K \times D}$ and those queries are updated via multiple self attention layers and cross attention layers, where the keys and values are linearly projected from unet feature of \mathbf{x} . For QFormer, we use 4 layers with 8 attention heads and hidden dimension of 256.

A.5 MATCHING TECHNIQUE

We have developed a technique to identify the specific region corresponding to an object’s representation based on composed images of that representation. For a given target object representation, we first random sample multiple images and encode them into object representations. For each image, we then replace one object representation with the target object representation and decode the mixed representations. The images generated from this composed representation may include the target object if it is appropriately encoded. To determine the object region, we measure the RGB variance between the generated images. Additionally, we use the original image containing the target object representation and select the region that closely matches the original. Finally, we combine two metrics—the variance and the distance to the original image—to accurately specify the region.

² <https://huggingface.co/stabilityai/sd-vae-ft-ema-original>

³ <https://ommer-lab.com/files/latent-diffusion/celeba.zip>

Conv $3 \times 3 \times 3 \times 128$, stride=1
BatchNorm2d
ReLU
Conv $3 \times 3 \times 128 \times 128$, stride=1
BatchNorm2d
ReLU
Conv $3 \times 3 \times 128 \times 128$, stride=1
BatchNorm2d
ReLU
Conv $3 \times 3 \times 128 \times 128$, stride=1
BatchNorm2d
ReLU
ResBlock $3 \times 3 \times 128 \times 128$, stride=1
BatchNorm2d
ReLU
ResBlock $3 \times 3 \times 128 \times 128$, stride=1
BatchNorm2d
ReLU
FC 4096×10

Table 5: Encoder Architecture used in attribute disentanglement.

Input Resolution	16
Input Channels	3
Output Resolution	16
Self Attention	Middle Layer
Base Channels	128
Channel Multipliers	[1,1,2,4]
# Heads	8
# Res Blocks / Layer	1

Table 8: Unet Encoder Architecture used in object disentanglement.

Input Resolution	16
Input Channels	4
β scheduler	Linear
Mid Layer Attention	Yes
# Res Blocks / Layer	2
# Heads	8
Base Channels	192
Attention Resolution	[1,2,4,4]
Channel Multipliers	[1,2,4,4]

Table 11: Generative Prior Architecture used in object disentanglement.

ReLU
Conv $3 \times 3 \times 128 \times 128$, stride=1
BatchNorm2d
ReLU
Conv $3 \times 3 \times 128 \times 128$, stride=1

Table 6: ResBlock in the Encoder

Input Resolution	16
Input Channels	3
Input Channels	4
β scheduler	Linear
Mid Layer Attention	Yes
# Res Blocks / Layer	2
# Heads	8
Base Channels	64
Attention Resolution	[1,2,4,4]
Channel Multipliers	[1,2,4,4]

Table 7: Decoder Architecture used in attribute disentanglement

Input Resolution	16
Input Channels	3
β scheduler	Linear
Mid Layer Attention	Yes
# Res Blocks / Layer	2
# Heads	8
Base Channels	64
Attention Resolution	[1,2,4,4]
Channel Multipliers	[1,2,4,4]

Table 10: Generative Prior Architecture used in attribute disentanglement.

Conv $3 \times 3 \times 3 \times 128$, stride=1
BatchNorm2d
ReLU
Conv $3 \times 3 \times 128 \times 128$, stride=1
BatchNorm2d
ReLU
Conv $3 \times 3 \times 128 \times 128$, stride=1
BatchNorm2d
ReLU
Conv $3 \times 3 \times 128 \times 128$, stride=1
BatchNorm2d
ReLU
ResBlock $3 \times 3 \times 128 \times 128$, stride=1
BatchNorm2d
ReLU
ResBlock $3 \times 3 \times 128 \times 128$, stride=1
BatchNorm2d
ReLU
FC 4096×10

Table 12: Encoder Architecture used in attribute disentanglement.

ReLU
Conv $3 \times 3 \times 128 \times 128$, stride=1
BatchNorm2d
ReLU
Conv $3 \times 3 \times 128 \times 128$, stride=1

Table 13: ResBlock in the Encoder

Input Resolution	16
Input Channels	4
β scheduler	Linear
Mid Layer Attention	Yes
# Res Blocks / Layer	2
# Heads	8
Base Channels	192
Attention Resolution	[1,2,4,4]
Channel Multipliers	[1,2,4,4]

Table 14: Generative Prior Architecture used in object disentanglement.

A.6 COMPUTING RESOURCES

We conduct all our experiments on a GPU Server consists of Intel Xeon Gold 6230 CPU, 256GB RAM, and 8 NVIDIA RTX 3090 GPUs (with 24GB VRAM), or 8 NVIDIA RTX 6000 GPUs (with 48GB VRAM). It takes about 24 GPU hours and from 36 to 48 GPU hours for attribute and object disentanglement experiment, respectively.